Chapter 19
Limited Influence of Sediment Grain Size on Elemental XRF Core Scanner Measurements

Sébastien Bertrand, Konrad Hughen and Liviu Giosan

Abstract X-ray fluorescence (XRF) scanning of sediment cores allows the rapid acquisition of bulk geochemical data at high resolution. The XRF core scanner data, which are expressed as elemental counts or peak areas, are mainly related to elemental concentrations, but they are also influenced by a series of sediment physical properties that vary with depth, such as bulk density, water content, organic matter content, and grain size. Here, we investigate the influence of grain size on elemental XRF peak areas by comparing ITRAX XRF core scanner measurements to ICP-AES elemental concentrations for two sediment cores with variable grain size. Results provide evidence for a limited influence of sediment grain size on XRF peak areas. This influence is negligible for sediment cores with grain-size variations of 10 μm or less. Our data also demonstrate that for cores with large grain-size variations, correcting the peak areas for water content improves the precision of the XRF measurements by a factor of three. This study therefore demonstrates that, for most sediment cores, the precision of data obtained by XRF core scanning is not significantly altered by grain-size variations.

Keywords Calibration · Grain size · Inorganic geochemistry · Sediment cores · Water content · ITRAX XRF core scanner

S. Bertrand (✉) · K. Hughen
Marine Chemistry and Geochemistry, Woods Hole Oceanographic Institution, Woods Hole, MA, USA
e-mail: sebastien.bertrand@ugent.be

S. Bertrand
Renard Centre of Marine Geology, Ghent University, Ghent, Belgium

L. Giosan
Geology and Geophysics, Woods Hole Oceanographic Institution, Woods Hole, MA, USA

I. W. Croudace, R. G. Rothwell (eds.), *Micro-XRF Studies of Sediment Cores*,
Developments in Paleoenvironmental Research 17, DOI 10.1007/978-94-017-9849-5_19

Introduction

XRF core scanning is increasingly used to generate geochemical records of sediment cores at high resolution. This non-destructive technique provides bulk sediment chemical data, expressed as elemental counts or peak areas. Although XRF measurements are mostly a function of elemental concentrations, they are also influenced by the characteristics of the X-ray source (energy level, nature of the tube) and detector (counting time), by core surface topography, and by a series of sediment physical properties such as bulk density, water content, organic matter content, and grain-size. Since these physical parameters frequently vary with depth in sediment cores, it is crucial to understand their effect on XRF geochemical data to better constrain the potential and limits of the method and avoid over-interpretation of the data.

Among those physical parameters, grain-size is thought to exert a strong influence on XRF peak areas (Croudace et al. 2006). In traditional WD-XRF analysis, the grain-size effect is reduced by grinding the sediment samples to homogenous sizes, generally below 60 μm (Injuk et al. 2006). Since XRF core scanners analyze raw sediment cores, downcore changes in grain-size distributions may significantly affect the results, especially for cores containing sand-size particles. In this study, we therefore investigated the influence of grain-size on elemental XRF peak areas by comparing ITRAX XRF measurements to ICP-AES concentrations obtained on two sediment cores with variable grain-size. We deliberately selected two cores from the same region, but with clearly distinct grain-size variations.

Material and Methods

Sediment Cores

The two sediment cores used in this study were collected in the fjords of Chilean Patagonia (Fig. 19.1; Bertrand et al. 2012b). Core JPC14 (46.449°S–73.798°W) is a 15 m long jumbo piston core collected at a depth of 129 m during cruise NBP05-05 on board RVIB Nathaniel B. Palmer. It is composed of a 3 m thick sand unit, surrounded by fine-grained sediment (Fig. 19.2). It covers the last 5400 years and essentially contains sediment delivered by a proglacial river system (Bertrand et al. 2012a). Accumulation rates vary between ~1 and ~10 mm/year (Bertrand et al. 2012a). In 2008, a complete core half was shipped from the Antarctic Marine Geology Research Facility of Florida State University, USA, to the Woods Hole Oceanographic Institution, MA, USA, for XRF core scanning and sub-sampling. Samples (3 cm^3) were taken every 10 cm with a plastic syringe (diameter 15 mm) for geochemical and water content analysis. Additional small (~0.1 cm^3) samples were taken every 2–4 cm for grain-size analysis, and kept wet in microcentrifuge tubes.

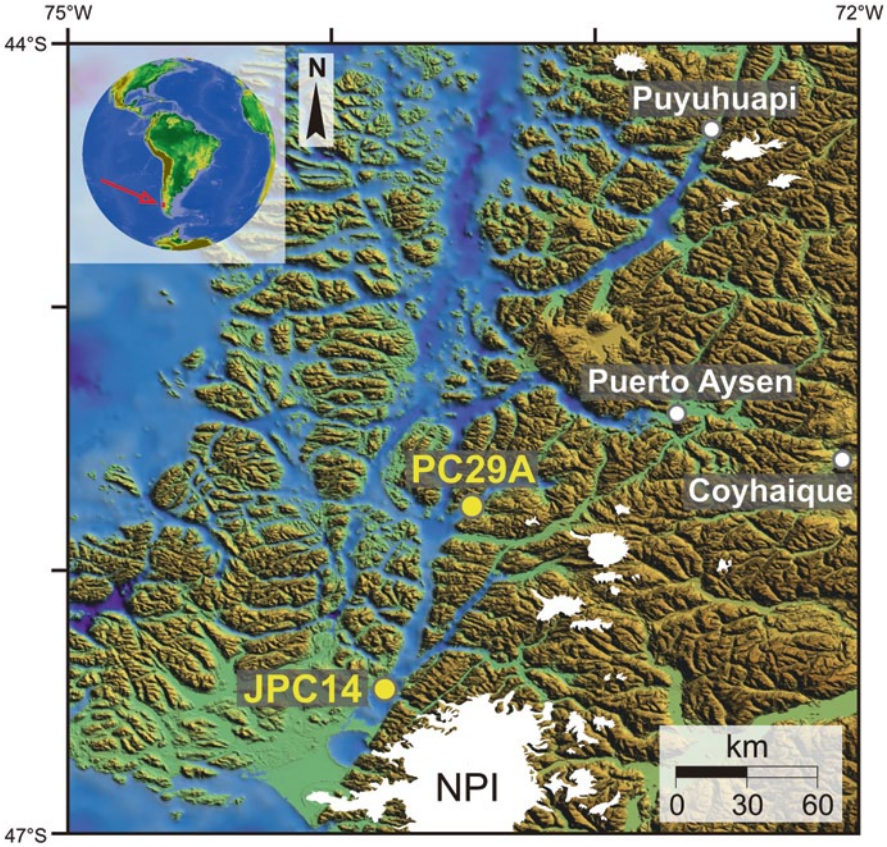

Fig. 19.1 Location of sediment cores JPC14 and PC29A in the fjords of Northern Chilean Patagonia. The location of the Northern Patagonian Icefield (NPI) and other ice masses is from Glasser et al. (2011)

Core PC29A (45.756°S–73.467°W) is a 208 cm long piston sediment core collected at a depth of 112 m during cruise Cimar Fiordo 7 (Fig. 19.1). It is entirely composed of fine-grained (silt) sediment and it represents the last 1400 years (Fig. 19.2; Bertrand et al. 2014). Accumulation rate is ~1–1.5 mm/year. One core half was sub-sampled in 1 cm thick slices for geochemical and water content analysis. Additional small (~0.1 cm^3) samples were taken every 4 cm in the second half for grain-size measurements.

The samples from both cores were freeze-dried and the wet and dry sample weights were recorded for water content calculation. Both cores are carbonate-free and contain low amounts of organic matter (TOC < 2 %) and biogenic opal (< 15 %).

XRF Core Scanning

The inorganic geochemistry of sediment cores JPC14 and PC29A was measured with an ITRAX XRF core scanner (Cox Analytical Instruments) at a resolution of 2 and 1 mm, respectively. The sediment surface was smoothed and covered with a 4 μm thin Chemplex 416 Prolene foil to avoid contamination of the XRF detector, prevent cross-contamination, and limit drying of the sediment during analysis. The scanner was operated with 20 s scan times using a Mo X-Ray tube set to 30 kV and 45 mA, which produces good excitation for a large range of elements of interest in geochemistry (Croudace et al. 2006; Cuven et al. 2007). The XRF spectra were interpreted and the peak areas quantified using software Q-Spec 6.5. For comparison with ICP-AES measurements, the XRF peak areas corresponding to the size of the sub-samples (10 or 15 mm) were averaged. In addition, pressed pellets of 102 non-ground freeze-dried samples of sediment core PC29A were scanned to assess the influence of grain-size on XRF peak areas without influence of bulk density and water content. The pellets were pressed at 20 t and they were scanned on the ITRAX XRF core scanner using the same configuration as for the wet sediment cores.

Wet Chemistry

A subset of 44 samples from core JPC14 and 102 samples from core PC29A was analyzed for inorganic geochemistry by ICP-AES. Samples were prepared using the Li-metaborate fusion technique of Murray et al. (2000), which is preferred over HF digestion because it is the only technique that allows the complete dissolution of sediment samples containing refractory minerals such as zircon (Sholkovitz 1990; Huang et al. 2007). Sample preparation consisted in mixing 200 ± 1.0 mg of ultrapure Li-metaborate (SCP Science) in 3 ml Pt:Au (95:5) crucibles, with 50 ± 0.5 mg of sediment. Ten microliter of 25 % LiBr were then added to the mixture and the crucibles were placed in a muffle furnace for 12 min at 1050 °C. The newly formed glass bead was then allowed to cool down for 2–3 min, detached from the crucible, and poured into a Teflon beaker containing a swirling 25 ml solution of 5 % HNO_3. Complete dissolution occurred within ~45 min. The solution was then filtered through a 0.45 μm PVDF Millipore filter and diluted in 5 % HNO_3 to obtain a 4000 x final dilution of the sample. The exact dilution factor was calculated from the precise weight of sediment used for fusion. Thirteen elements were measured on a JY Ultima C ICP-AES. Analytical details are given in Bertrand et al. (2012b).

Grain-Size

Grain-size was measured on the terrigenous fraction of the sediment using a Coulter LS200 laser particle size analyzer. To isolate the terrigenous fraction, samples were

treated with boiling H_2O_2, HCl, and NaOH to remove organic matter, eventual carbonates, and biogenic silica respectively. No diatoms were observed in core JPC14, so the alkaline treatment was only applied to core PC29A. Prior to analysis, samples were boiled with 300 mg of sodium pyrophosphate ($Na_4P_2O_7 \cdot 10H_2O$) to ensure complete disaggregation of the particles. The grain-size distribution of the samples was measured during 90 s intervals and the arithmetic mean was calculated from the 92 size classes.

Results and Discussion

Lithology, Grain-Size, Water Content and Elemental Concentrations

Core JPC14 is essentially composed of three lithological units separated by relatively abrupt transitions (Fig. 19.2a). It is composed of fluvio-glacial silts (~20 μm) at 0–740 cm and 1109–1500 cm, and of poorly sorted sand (80–120 μm) at 800–1086 cm (Bertrand et al. 2012a). The water content of the sediment is negatively correlated to grain-size, with high water content (45–50 %) in fine-grained samples and low water content (20–30 %) in the sand unit (Figs. 19.2 and 19.3). The few exceptions are the low water content silt layers in the upper 2 m of the sediment core. The lower water content of the sand unit is due to the combination of low porosity in poorly sorted sands (e.g., Syvitski 2007) and faster dewatering of coarse deposits.

The grain-size of core PC29A gradually evolves from medium to fine silt (16–31 μm; Fig. 19.2b). The water content is rather constant (47–53 %) and it shows no relation to grain-size (Fig. 19.3). By comparison, the range of grain-size variations in core JPC14 is 12 times higher than for core PC29A (Table 19.1 in Appendix; Fig. 19.3).

Both cores are essentially composed of alumino-silicates that originate from the mixing of slightly weathered granodiorites and North Patagonian andosols (Bertrand et al. 2012b). The chemical composition of the two sediment cores is roughly similar, albeit much more variable for core JPC14 (Table 19.1 in Appendix). Some elements such as Sr and Zr are clearly enriched in the coarse unit of core JPC14, while K and Fe are concentrated in fine-grained sediments (Figs. 19.2 and 19.4; Bertrand et al. 2012b), in agreement with the observations of Cuven et al. (2010). For core PC29A, Ti and Fe concentrations are ~25 and ~15 % higher in fine silts than in coarse silts, respectively (Fig. 19.5).

Relation Between XRF Peak Areas and Elemental Concentrations

XRF peak areas and elemental concentrations, as measured by ICP-AES, show significant positive correlations for most elements (Figs. 19.4 and 19.5). Correla-

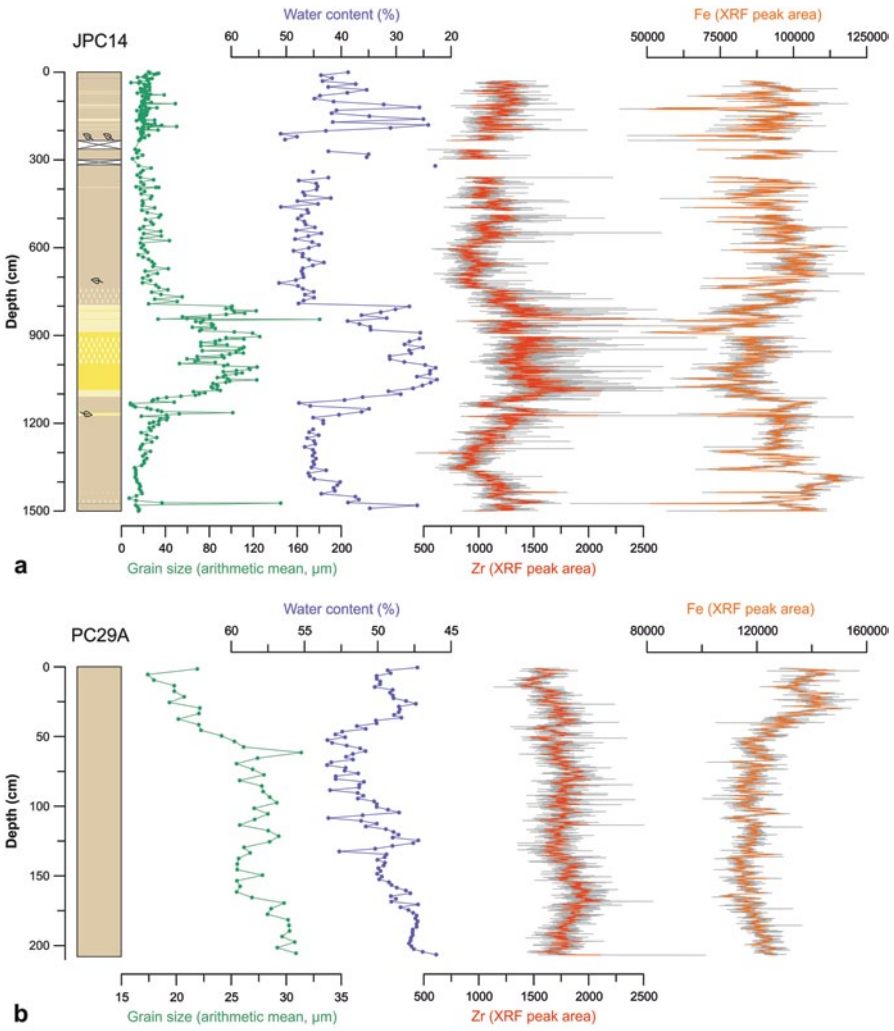

Fig. 19.2 Lithology of sediment cores JPC14 and PC29A, and downcore variations in grain-size, water content, and selected geochemical elements. (From Bertrand et al. 2012a, 2014)

tions are better for heavy and abundant elements such as Ca and Fe (Table 19.2 in Appendix), as previously observed (Croudace et al. 2006; Richter et al. 2006; Tjallingii et al. 2007). The light elements Al and Si show no significant correlation, even though these elements are well above their theoretical detection limit (~10,000 ppm, Cox Analytical Systems, technical documentation). One of the reasons is that the XRF radiation for these elements is heavily absorbed by the variable water film that forms between the sediment surface and the covering plastic foil (Kido et al. 2006; Tjallingii et al. 2007). Since fjord sediments are deposited in environments of highly variable salinity, using chlorine to correct the XRF peak areas for absorption by the interstitial water layer, as proposed by Tjallingii et al.

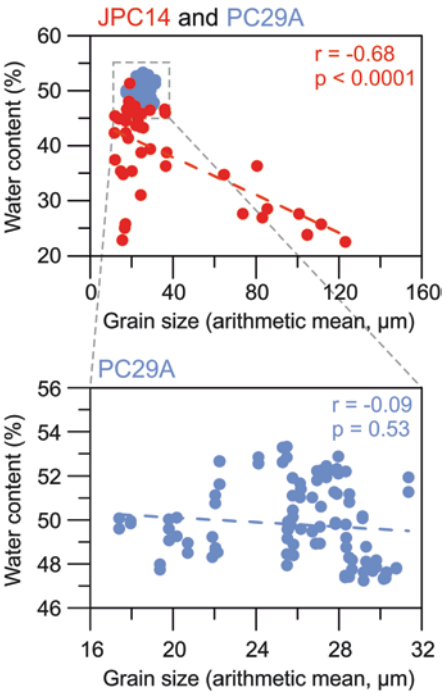

Fig. 19.3 Correlation plots between water content and grain-size. Note the significant negative correlation for core JPC14 (*red dots*) and the absence of correlation for core PC29A (*blue*). The four JPC14 data points corresponding to low grain-size and low water content values represent unusual silt layers in the upper part of the sediment core. (see Fig. 19.2)

(2007), does not improve the correlations for Al and Si. For the XRF data obtained on pressed pellets, the correlation coefficients between XRF peak areas and ICP-AES elemental concentrations are better for all elements except Sr (Table 19.2 in Appendix; Fig. 19.5). This is in contrast with Tjallingii et al. (2007), who found that the improvement of the correlation coefficients mainly concerned light elements (Al and Si).

Assessing the Influence of Grain-Size Variations on XRF Peak Areas

To assess the influence of sediment grain-size on XRF core scanner peak areas, we compared the normalized ratio between XRF peak area and ICP-AES concentration (hereafter XRF/ICP) to sediment grain-size for both cores. Normalization consisted in dividing the XRF peak area to ICP-AES concentration ratio by the average value of this ratio for each core. If grain-size has an influence on XRF intensities, the XRF/ICP values should be significantly correlated to grain size.

Core JPC14

For core JPC14, which presents high variations in grain-size, the XRF/ICP ratio of most elements shows a weak positive correlation with grain-size (Fig. 19.6a). This

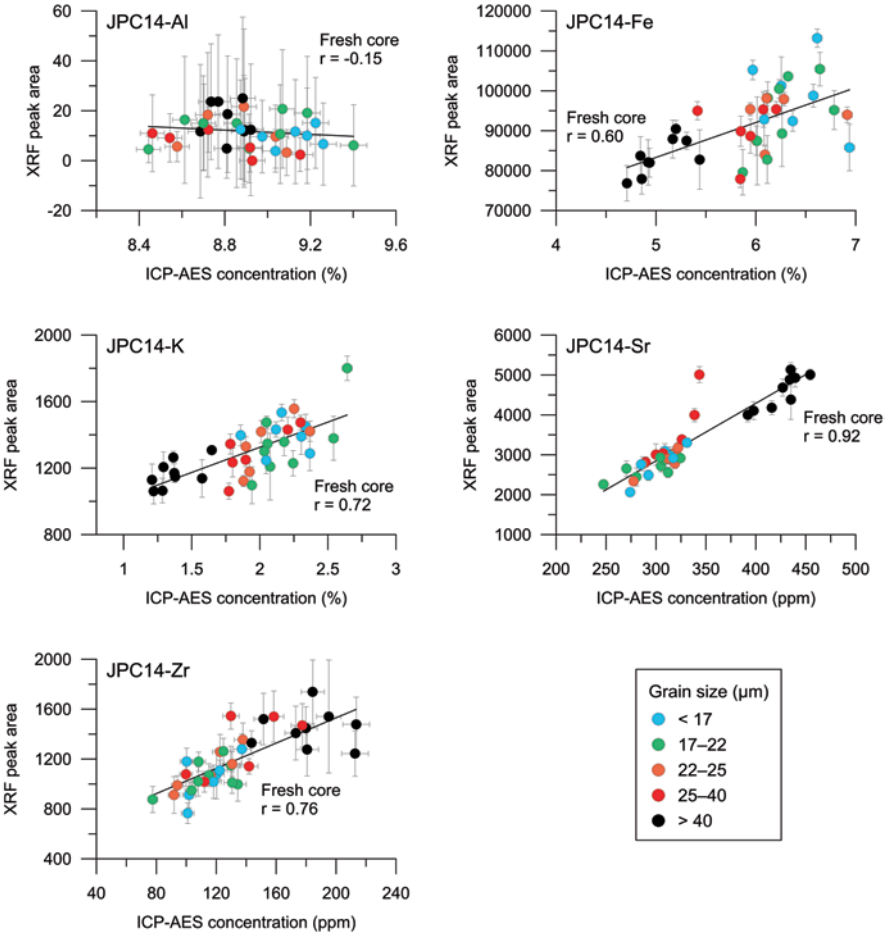

Fig. 19.4 Correlations between ITRAX XRF core scanner peak areas and ICP-AES concentrations for selected elements measured on sediment core JPC14 ($n = 37$). The *error bars* represent 1 sigma

relation is significant for K, Ti, Fe, and Sr (Table 19.3a in Appendix). Only Zr shows a statistically significant negative correlation. The absolute values of the slopes of the significant correlations reach $1.2–4.3 \times 10^{-3}$, i.e., an increase of the XRF peak areas of 0.1% per micron for Ti and Fe, of 0.2% per micron for Sr, of 0.4% per micron for K, and a decrease of 0.2% per micron for Zr (Table 19.3 in Appendix).

Since the water content of core JPC14 is tightly linked to grain-size ($r = -0.68$, $p < 0.0001$, see Fig. 19.3), a significant negative correlation is also observed between XRF/ICP and water content for most elements (Fig. 19.6b, Table 19.3b in Appendix). This reflects a general decrease of the XRF peak areas with increasing water content. Except for Ti, the significant correlations concern the same elements as for the correlations between XRF/ICP and grain-size (Table 19.3 in Ap-

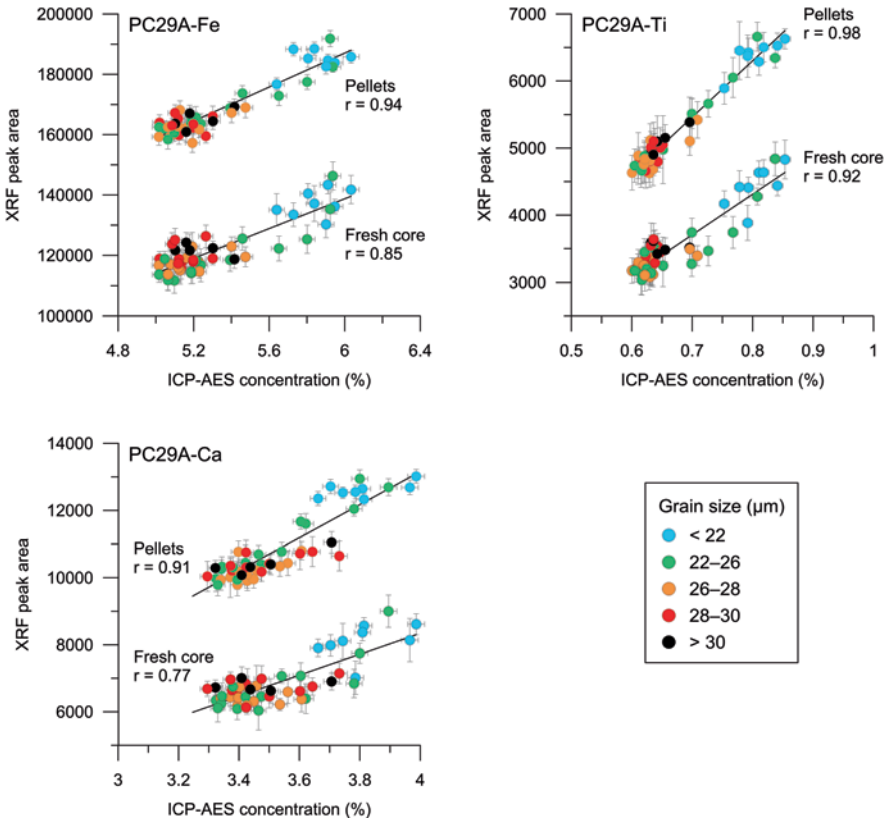

Fig. 19.5 Correlations between ITRAX XRF core scanner peak areas and ICP-AES concentrations for selected elements measured on sediment core PC29A ($n = 51$). The plots show results obtained on wet sediment and on pressed pellets (see Core PC29A for details). The *error bars* represent 1 sigma

pendix). This demonstrates that changes in water content are responsible for part of the observed variability in XRF peak areas. This observation also highlights the potential of water content data to correct XRF peak areas obtained on sediments of highly variable grain-size.

For core JPC14, correcting the XRF peak areas for water content (using the linear regressions displayed in Fig. 19.6b) reduces the slopes of the XRF/ICP versus grain-size relations by 60–85 % (Table 19.3c and d in Appendix; Fig. 19.7). After water content correction, the XRF/ICP ratios of all elements but K lose their significant correlation to grain-size (Table 19.3c in Appendix), which means that after water content correction, the relations between XRF peak areas and elemental concentrations are mostly independent of grain-size variations. For sediments of highly variable grain-size, such as those of core JPC14, correcting XRF peak areas for water content therefore significantly reduces the apparent influence of grain-size on XRF peak areas.

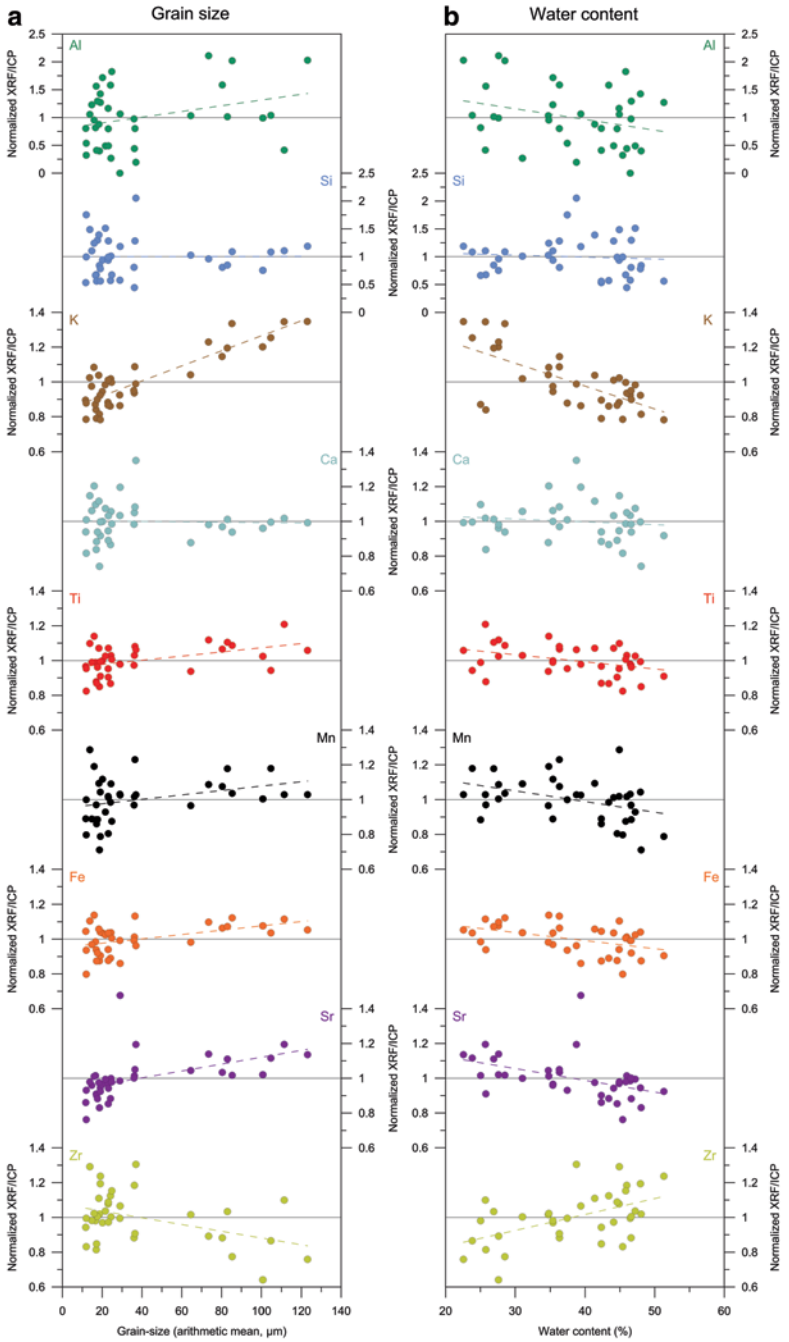

Fig. 19.6 Correlations between normalized XRF peak areas/ICP-AES concentrations and (**a**) grain-size, or (**b**) water content for geochemical elements measured on sediment core JPC14. Note the vertical scale difference between Si–Al and the other elements. (0–2.5 for Si and Al and 0.6–1.4 for the other elements)

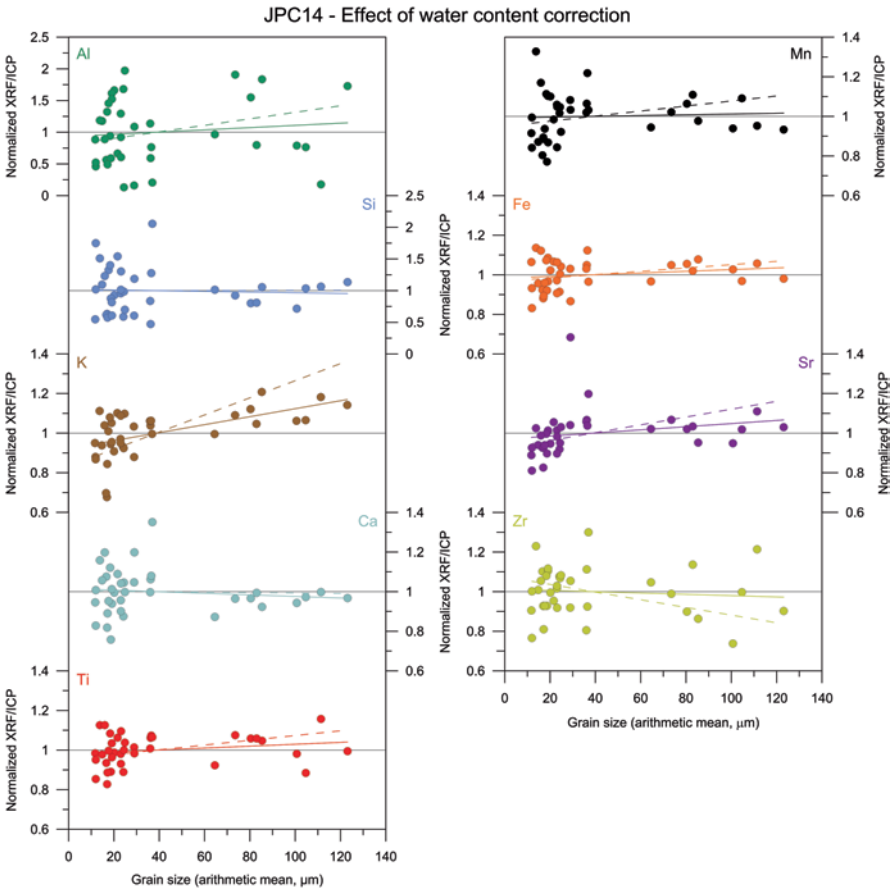

Fig. 19.7 Correlations between normalized XRF peak areas corrected for water content/ICP-AES concentrations and grain-size for geochemical elements measured on sediment core JPC14. The correlations corresponding to water content-corrected measurements are represented by *continuous lines*, while those corresponding to raw measurements are shown as *dashed lines*, as in Fig. 19.6a. The water content correction is derived from the linear regressions presented in Fig. 19.6b. Geometrically, correcting the JPC14 data for water content corresponds to flattening the trends shown in Fig. 19.6b. Note the general decrease in the slope of the correlation lines after water content correction, except for Si and Ca

Overall, correcting the XRF peak areas for either water content or grain-size slightly improves the correlation between XRF peak areas and ICP concentrations (Table 19.4 in Appendix). This improvement is however relatively minor, and the difference between the correlation coefficients is never significant at $p < 0.05$ (Fisher's transformation test). We particularly note that the correlations between XRF peak areas and elemental concentrations for Al and Si remain insignificant after correction.

Core PC29A

For core PC29A, which shows minor grain-size variations compared to core JPC14, the relations between XRF/ICP and grain-size are insignificant for most elements, and the sign of the relation varies inconsistently among elements (Fig. 19.8a; Table 19.5a in Appendix). The relation is only significant for Ca, Mn and Sr (Table 19.5a in Appendix). The absolute values of the slopes vary between 0.53 and 8.98 (Table 19.5a in Appendix), which represent fluctuations of the XRF peak areas of 0.05–0.9 % per micron.

Since the water content of core PC29A is rather stable and that it is not significantly correlated to grain-size, the Pearson correlation coefficients between the XRF/ICP ratios and water content are also weak and the significant correlations relate to different elements (Fig. 19.8b, Table 19.5b in Appendix). Therefore, correcting the XRF peak areas obtained for core PC29A for water content does not decrease the number of significant correlations with grain-size or the slope of the correlations (Table 19.5c in Appendix). Correcting the PC29A XRF peak areas for water content therefore does not render the data less dependent on grain-size.

To focus on the influence of grain-size and avoid the influence of other physical properties such as bulk density, correlations between XRF/ICP and grain-size were also calculated for the XRF data obtained on dry pellets. These pressed pellets have a constant bulk density and they contain no water. It is therefore expected that grain-size is the main physical parameter influencing the XRF peak areas. The results are rather similar to what was obtained for the wet sediment core (Table 19.5d in Appendix). The influence of grain-size on XRF peak areas is only significant for elements Ca, Fe, and Sr, which demonstrates that the effect of grain-size on the XRF peak areas of core PC29A is limited, and insignificant for most elements. The absolute values of the slopes reach values of 0.3–10.9, which are of the same order of magnitude than for the measurements obtained on wet sediment cores.

In summary, the PC29A dataset shows that grain-size variations significantly affect the XRF peak areas of a few elements only, and that these variations are on the order of 0–1 % per micron. There is however no consistency in the level of imprecision caused by grain-size variations. Since the correlations between XRF peak areas and ICP-AES concentrations are significantly improved when using pressed pellets (Table 19.2 in Appendix), other physical properties such as bulk density must play an important role in the relatively high imprecision of XRF measurements obtained on wet sediment cores. Changes in bulk density are generally related to sediment packing, i.e., porosity, rather than grain density, and could be estimated using core logging of gamma-ray (e.g., Zolitschka et al. 2001) or x-ray (Francus et al., this volume) attenuation.

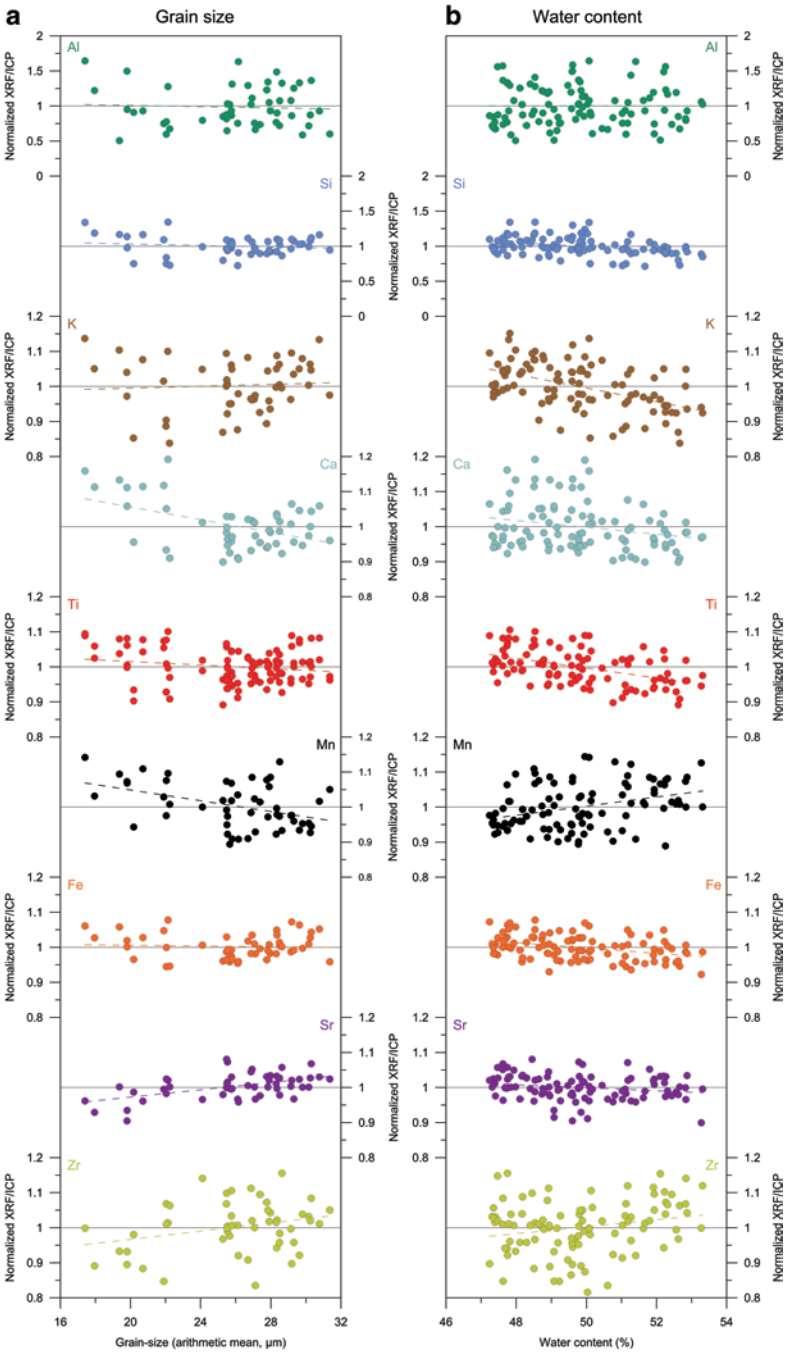

Fig. 19.8 Correlations between normalized XRF peak areas/ICP-AES concentrations and (**a**) grain-size, or (**b**) water content for geochemical elements measured on sediment core PC29A. Note the vertical scale difference between Si–Al and the other elements. (0–2 for Si and Al and 0.8–1.2 for the other elements)

Quantifying the Influence of Grain-Size Variations on XRF Peak Areas

In Table 19.6 (in Appendix), the slopes of the correlations between the XRF/ICP ratio and grain-size are used to quantify the effect of grain-size variations on XRF peak areas. The strongest significant imprecisions caused by changes in sediment grain-size are for elements K, Sr and Zr, on sediment core JPC14, and for elements Ca and Mn on sediment core PC29A. These imprecisions on peak areas caused by grain-size are always lower than 1 % per micron.

If we consider that imprecisions of 5 % are satisfactory, which is acceptable in elemental geochemistry (e.g., De Vivo et al. 2008), the results obtained on core JPC14 show that XRF peak areas obtained on sediment cores with grain-size variations of up to 20–40 μm. do not need to be corrected for grain-size. This value is however lower when considering the results obtained on core PC29A, for which an imprecision of 5 % corresponds to grain-size variations of as little as 6 μm for some elements.

For Fe and Ti, which are among the most frequently used elements in XRF studies of sediment cores, grain-size variations of up to 40 μm do not affect the XRF peak areas for more than 5 %. For cores that present large grain-size variations, such as JPC14, correcting the XRF peak areas for water content significantly improves the precision, and therefore increases the grain-size range for which good XRF data can be obtained, by a factor of three.

Conclusions

The comparison between XRF core scanner peak areas and ICP-AES elemental concentrations obtained on sediment cores JPC14 and PC29A provides evidence for a limited influence of sediment grain-size variations on XRF peak areas. Grain-size variations only affect a limited but inconsistent number of elements. For the elements that are affected, the effect of grain-size is negligible for grain-size ranges of 10–20 μm. For cores that show large variations in grain-size, correcting the peak areas for water content variations improves the precision of the XRF core scanner data by a factor of three. This study therefore demonstrates that grain-size variations are not a major issue in XRF core scanning of sediment cores. Further studies should focus on assessing the influence of other sediment physical properties, e.g., bulk density, on XRF peak areas.

Acknowledgments This research was supported by an EU FP6 Marie Curie Outgoing Fellowship to S.B. Cruise NBP0505 was funded by the US National Science Foundation, Office of Polar Programs grant number NSF/OPP 03-38137 to J. Anderson (Rice University) and J. Smith Wellner (University of Houston). The Cimar-7 Program was supported by the Chilean National Oceanographic Committee (CONA, Grant C7F 01-10 to S. Pantoja). We thank the curators of the Florida State University Antarctic Marine Geology Research Facility (Simon Nielsen and Lindsey Geary) for their assistance with shipping core JPC14 to WHOI. We are grateful to Jess Tierney (WHOI) for her help with the XRF core scanner measurements, and to Jan-Berend Stuut and Inka Meyer (MARUM, Bremen, Germany) for providing access to the Coulter particle size analyzer. S.B. is currently a postdoctoral fellow of the Flemish Research Foundation (FWO, Belgium).

Appendix

Table 19.1 Descriptive statistics (arithmetic mean, minimum and maximum) of grain-size, water content and ICP-AES elemental concentrations for cores JPC14 (n geochemistry = 44) and PC29A (n geochemistry = 102). The relative range (r.r., or range percent variation, i.e., range divided by mean) is indicated in parentheses

	JPC14		PC29A	
	Mean	Min-max	Mean	Min-max
Grain-size (μm)	40.1	7.1–180.4 *(n = 319)*	26.0	17.4–31.4 (*n* = 51)
Water content (%)	39.9	22.6–51.3 *(n = 141)*	49.7	47.2–53.3 *(n = 102)*
Al (wt.%)	8.87	8.44–9.40 *(r.r. = 10.8%)*	7.80	7.59–8.21 *(r.r. = 8.0%)*
Si (wt.%)	26.4	24.4–29.4 *(r.r. = 19.1%)*	25.0	23.8–25.9 *(r.r. = 8.5%)*
K (wt.%)	1.93	1.21–2.64 *(r.r. = 74.3%)*	1.32	1.20–1.42 *(r.r. = 16.7%)*
Ca (wt.%)	3.47	2.60–4.41 *(r.r. = 52.2%)*	3.53	3.20–4.02 *(r.r. = 23.4%)*
Ti (wt.%)	0.62	0.55–0.66 *(r.r. = 18.1%)*	0.68	0.60–0.85 *(r.r. = 37.4%)*
Mn (wt.%)	0.108	0.089–0.130 *(r.r = 38.5%)*	0.093	0.086–0.103 *(r.r = 18.2%)*
Fe (wt.%)	5.93	4.71–6.94 *(r.r. = 37.6%)*	5.35	4.94–6.14 *(r.r. = 22.6%)*
Sr (ppm)	332	247–454 *(r.r. = 62.3%)*	385	350–430 *(r.r. = 20.6%)*
Zr (ppm)	135	78–213 *(r.r. = 101.0%)*	183	159–210 *(r.r. = 28.1%)*

Table 19.2 Pearson correlation coefficients (*r*) between elemental XRF core scanner peak areas and ICP-AES concentrations. The XRF measurements were obtained on fresh sediment cores for (a) and (b) and on dry pressed pellets for (c). Values in bold indicate correlations that are significant at $p < 0.01$. The elements are ranked by atomic number. Correlation plots for selected elements are represented in Figs. 19.4 and 19.5. The low values of r for Ti in JPC14, and for K and Zr in PC29A are due to the low range of concentrations of these elements in these specific cores (see Table 19.1). Because not all variables are normally distributed, especially for core PC29A (Shapiro-Wilk test), Spearman correlation coefficients were also calculated. The results show no change in the significance of the correlations at $p < 0.01$

Element	Atomic number	(a) JPC14	(b) PC29A	(c) Pellets PC29A
Al	13	−0.15	−0.03	0.22
Si	14	0.34	−0.10	**0.33**
K	19	**0.72**	−0.03	**0.49**
Ca	20	**0.77**	**0.77**	**0.91**
Ti	22	0.26	**0.92**	**0.98**
Mn	25	0.37	**0.72**	**0.81**
Fe	26	**0.60**	**0.85**	**0.94**
Sr	38	**0.92**	**0.71**	**0.57**
Zr	40	**0.76**	0.21	**0.37**
n	–	*37*	*102*	*102*

Table 19.3 Pearson correlation coefficients (r) and slopes of the linear regressions ($\times 10^3$) between normalized XRF peak areas/ICP concentrations and (a) grain-size, or (b) water content, for sediment core JPC14 ($n = 37$). See graphical representation in Fig. 19.6. Values in bold indicate correlations that are significant at $p < 0.01$. The slope values in gray indicate the elements for which correlations are not significant at $p < 0.01$. Note the opposite signs of the regressions between (a) and (b) for most elements. Higher absolute values of the slopes indicate a higher influence of (a) grain-size or (b) water content variations on XRF core scanner peak areas. Correcting the XRF peak areas for water content (c) decreases the significance and the absolute values of the slopes of the correlations between XRF peak areas/ICP concentrations and grain-size. The relative decrease in the slope is indicated in (d). The water content correction consisted in back-calculating the XRF peak area/ICP concentration values using the regressions shown in Fig. 19.6b. See illustration in Fig. 19.7

JPC14	(a) Grain size		(b) Water content		(c) Grain size after water content correction		(d) Relative decrease in slope after water content correction (%)
Element	r	slope	r	slope	r	slope	
Al	0.30	5.14	–0.29	–19.2	0.11	1.76	66
Si	0.01	0.06	–0.08	–3.44	–0.05	–0.54	–
K	***0.87***	4.32	***–0.69***	–13.1	***0.56***	2.02	53
Ca	–0.03	–0.01	–0.12	–1.61	–0.11	–0.40	–
Ti	***0.45***	1.2	–0.40	–4.10	0.19	0.48	60
Mn	0.32	1.27	–0.40	–3.06	0.05	0.19	85
Fe	***0.47***	1.24	***–0.46***	–4.65	0.18	0.43	65
Sr	***0.51***	1.98	***–0.45***	–6.77	0.23	0.79	60
Zr	***–0.43***	–1.94	**0.52**	9.17	–0.08	–0.33	83
							mean = 69

Table 19.4 Pearson correlation coefficients (r) between elemental XRF core scanner peak areas and ICP-AES concentrations before any correction (a), after water content correction only (b), and after grain-size correction only (c), for sediment core JPC14 ($n = 37$). Values in bold indicate correlations that are significant at $p < 0.01$. The low values of r for Ti are due to the low range of Ti concentrations in core JPC14 (relative range of 18.1%, see Table 19.1). Correcting the XRF peak areas for water content or grain-size, using the regressions shown in Fig. 19.6, does not significantly increase the correlation coefficients between elemental XRF core scanner peak areas and ICP-AES concentrations. (Fisher r-to-z transformation, two-tailed test, $p < 0.05$)

JPC14	Correction		
Element	(a) None	(b) Water content	(c) Grain-size
Al	−0.15	−0.21	−0.08
Si	0.34	0.27	0.25
K	*0.72*	*0.81*	*0.81*
Ca	*0.77*	*0.74*	*0.78*
Ti	0.26	0.30	0.19
Mn	0.37	*0.50*	*0.56*
Fe	*0.60*	*0.73*	*0.72*
Sr	*0.92*	*0.87*	*0.85*
Zr	*0.76*	*0.86*	*0.85*

Table 19.5 Pearson correlation coefficients (r) and slopes of the linear regressions ($\times 10^3$) between normalized XRF peak areas/ICP concentrations and (a) grain-size, or (b) water content, for sediment core PC29A [$n = 51$ for (a) and 102 for (b)]. See graphical representation in Fig. 19.8. Values in bold indicate correlations that are significant at $p < 0.01$. The slope values in gray indicate the elements for which correlations are not significant at $p < 0.01$. Higher absolute values of the slopes indicate a higher influence of (a) grain-size or (b) water content variations on XRF core scanner peak areas. Correcting the XRF peak areas for water content (c) does not systematically decrease the slope of the regressions. Column (**d**) represents the Pearson correlation coefficients (r) and slopes of the linear regressions ($\times 10^3$) between normalized XRF peak areas obtained on pressed pellets/ICP concentrations and grain-size ($n = 51$). The relative change in the slope of the linear regressions between data obtained on dry pellets (d) and fresh sediment cores (a) is indicated in (e). The results show that, for core PC29A, XRF data obtained on pressed pellets are not more or less dependent on grain-size than data obtained on fresh sediment cores

PC29A	(a) Grain size		(b) Water content		(c) Grain size after water content correction		(d) Grain size - pressed pellets		(e) Relative change in slope after correction (%)
Element	r	slope	r	slope	r	slope	r	slope	
Al	–0.05	–4.36	–0.07	–0.02	–0.01	–1.06	–0.30	–8.51	–95
Si	–0.14	–5.39	***–0.34***	–2.82	***–0.27***	–9.43	–0.24	–2.20	59
K	0.06	1.33	***–0.48***	–19.5	***–0.05***	–0.80	0.11	1.19	11
Ca	***–0.46***	–8.98	–0.24	–9.88	–0.56	–10.67	***–0.78***	–10.88	–21
Ti	–0.13	–1.95	***–0.49***	–14.0	***–0.25***	–3.06	–0.33	–2.46	–26
Mn	***–0.42***	–7.68	***0.35***	13.0	***–0.25***	–4.24	–0.10	–0.58	92
Fe	–0.05	–0.53	***–0.39***	–7.59	***–0.07***	–0.66	***0.37***	0.32	40
Sr	***0.52***	5.20	–0.21	–4.31	0.46	4.64	***0.51***	5.65	–9
Zr	0.29	5.84	0.22	9.97	0.49	10.57	0.35	7.44	–27
									mean = 3

Table 19.6 Decrease in the relative precision of XRF core scanner measurements due to grain-size variations, for data obtained on sediment core JPC14 before (a), and after (b) water content correction, and for data obtained on sediment core PC29A (c). These values are derived from the slope of the linear regressions presented in Figs. 19.6a, 19.7 and 19.8a. Columns (d) to (f) present the range of grain-sizes that corresponds to a relative precision of XRF core scanner measurements of 5 %. (see Tables 19.3a, 19.3c and 19.5a)

Element	Decrease in relative precision per micron (%)			Range of grain-sizes corresponding to 5 % precision (μm)		
	(a) JPC14	(b) JPC14-corrected for water content	(c) PC29A	(d) JPC14	(e) JPC14-corrected for water content	(f) PC29A
Al	–	–	–	–	–	–
Si	–	–	–	–	–	–
K	0.43	0.20	–	12	25	–
Ca	–	–	0.90	–	–	6
Ti	0.12	–	–	42	–	–
Mn	–	–	0.77	–	–	7
Fe	0.12	–	–	40	–	–
Sr	0.20	–	0.52	25	–	10
Zr	0.19	–	–	26	–	–

"–" indicates elements for which the influence of grain-size on XRF peak areas is insignificant at $p < 0.01$

References

Bertrand S, Hughen KA, Lamy F, Stuut JBW, Torréjon F, Lange CB (2012a) Precipitation as the main driver of Neoglacial fluctuations of Gualas glacier, Northern Patagonian Icefield. Clim Past 8:519–534

Bertrand S, Hughen K, Sepúlveda J, Pantoja S (2012b) Geochemistry of surface sediments from the fjords of Northern Chilean Patagonia (44–47°S): spatial variability and implications for paleoclimate reconstructions. Geochim Cosmochim Acta 76(1):125–146

Bertrand S, Hughen KA, Sepúlveda J, Pantoja S (2014) Late Holocene covariability of the southern westerlies and sea surface temperature in northern Chilean Patagonia. Quat Sci Rev 105, 195–208

Croudace IW, Rindby A, Rothwell RG (2006) ITRAX: description and evaluation of a new multi-function X-ray core scanner. In: Rothwell RG (ed) New techniques in sediment core analysis. Geol Soc Spec Publ 267:51–63

Cuven S, Francus P, Cremer J-F (2007) Protocoles d'utilisation et essais de calibration du scanner de microfluorescence X de type "ITRAX core scanner". INRS-ETE, Québec, rapport de recherche no 954, p 108

Cuven S, Francus P, Lamoureux SF (2010) Estimation of grain-size variability with micro X-ray fluorescence in laminated lacustrine sediments, cape bounty, Canadian high arctic. J Paleolimnol 44(3):803–817

De Vivo B, Belkin HE, Lima A (2008) Environmental geochemistry: site characterization, data analysis and case histories. Elsevier, Amsterdam, p 429

Glasser NF, Harrison S, Jansson KN, Anderson K, Cowley A (2011) Global sea-level contribution from the Patagonian icefields since the little ice age maximum. Nat Geosci 4:303–307

Huang S, Sholkovitz E, Conte M (2007) Application of high-temperature fusion for analysis of major and trace elements in marine sediment trap samples. Limnol Oceanogr Methods 5:13–22

Injuk J, Van Grieken R, Blank A, Eksperiandova L, Buhrke V (2006) Specimen preparation. In: Beckhoff et al (eds) Handbook of practical X-ray fluorescence analysis. Heidelberg, Springer, pp 411–429

Kido Y, Koshikawa T, Tada R (2006) Rapid and quantitative major element analysis method for wet fine-grained sediments using an XRF microscanner. Mar Geol 229:209–225

Murray R, Miller D, Kryc K (2000) Analysis of major and trace elements in rocks, sediments, and interstitial waters by inductively coupled plasma atomic emission spectrometry (ICP-AES). ODP Technical Note 29

Richter TO, van der Gaast S, Koster B, Vaars A, Giele R, de Stigte HC, De Haas H, van Weering TCE (2006) The avaatech XRF core scanner: technical description and applications to NE Atlantic sediments. In: Rothwell RG (ed) New techniques in sediment core analysis, vol 267. Geological Society Special Publication, London, pp 39–50

Sholkovitz E (1990) Rare-earth elements in marine sediments and geochemical standards. Chem Geol 88(3–4):333–347

Syvitski JPM (2007) Principles, methods and applications of particle size analysis, 3rd edn. Cambridge University Press, New York, p 388

Tjallingii R, Röhl U, Kölling M, Bickert T (2007). Influence of the water content on X-ray fluorescence core scanning measurements in soft marine sediments. Geochem Geophys Geosystems 8(2). doi:10.1029/2006GC001393

Zolitschka B, Mingram J, van der Gaast S, Jansen JHF, Naumann R (2001) Sediment logging techniques. In: Last WM, Smol JP (eds) Tracking environmental change using lake sediments, vol 1. Kluwer Academic, Dordrecht, pp 137–153